INFRARED IMAGES OF THE SUN DURING THE JULY 11, 1991 SOLAR ECLIPSE

E. V. TOLLESTRUP and G. G. FAZIO
Smithsonian Astrophysical Observatory, Cambridge, MA 02138, U.S.A.
J. WOOLAWAY and J. BLACKWELL
Amber Engineering, Inc., Santa Barbara, CA 93117, U.S.A.
and
K. BRECHER
Department of Astronomy, Boston University, Boston, MA 02215, U.S.A.

Abstract. Infrared images (1.65 μm) of the eclipsed Sun were taken atop Mauna Kea, Hawaii, during the July 11, 1991 total eclipse with an Amber Engineering 128×128 InSb array camera. The camera, mounted on a portable solar tracker, had a 3.8-cm, f/2 objective that produced a 4.9° field of view. The primary objective of the experiment was to search for dust or rocky rings around the Sun, previously detected at about 4 $R_\odot$. High thin clouds, atmospheric dust and aerosols from the June 1991 explosion of Mount Pinatubo in the Philippines, and the overall brightness of the solar corona resulted in a very high infrared background. Despite this, high signal-to-noise radial infrared intensity profiles were obtained of the solar corona from the Moon's limb out to about 10 $R_\odot$. Preliminary analysis shows some evidence for an enhanced surface brightness between 3 to 4 $R_\odot$ along the east-west direction, but much fainter than seen in previous solar eclipses. The transition region between the K-corona and the F-corona clearly shows at 2.5 $R_\odot$, and the surface brightness of the F-corona as a function of radius (from about 2 to 10 $R_\odot$) can be fit by a simple power law.

Key words: eclipses – infrared: stars – interplanetary medium – Sun: corona

1. Introduction

The detection of possible dust rings around the Sun has been an "on again, off again" affair ever since they were first reported in 1967. During the 1966 solar eclipse, Peterson (1967) and MacQueen (1967) independently detected excess 2.2 μm emission along the solar equatorial direction at a radius of about 4 $R_\odot$. MacQueen (1967) verified his results in 1967 by using a stratospheric balloon-borne coronagraph to scan the corona. Peterson found a broad emission peak with a maximum near 3.3 $R_\odot$ and a sharp peak at 3.9 $R_\odot$. MacQueen found two components during the 1966 eclipse, one at 3.5 and one at 4 $R_\odot$. During the 1967 balloon experiment, MacQueen detected peaks at 4, 8.7, and 9.2 $R_\odot$. These early results show clear evidence of enhanced infrared emission. But despite this, the more recent results have been ambiguous. Detections have been reported at 10 μm for the 1973 solar eclipse (Lena *et al.* 1974) and at several wavelengths for a multi-wavelength (1.25, 1.65, 2.25, and 2.8 μm) eclipse experiment in 1983 (Mizutani *et al.* 1984; Isobe *et al.* 1985). However, these results are not consistent with the 1966-67 results. The eclipse experiments in 1970, 1978, and 1980 have all been unsuccessful in finding dust rings (*e.g.*, Mankin *et al.* 1974; Peterson 1971; and Rao *et al.* 1981).

The solar corona is extremely bright and spatially complex, which makes these type of observations (scanned photometers) difficult. Not only do the K- and F-coronae overlap, but they have radial surface brightness profiles that are both steep

D. M. Rabin et al. (eds.), Infrared Solar Physics, 179–183.

https://doi.org/10.1017/S0074180900124416 Published online by Cambridge University Press

and varying. More troublesome are the solar streamers. They are very complicated, 3-dimensional structures which can only be viewed in projection as a 2-dimensional image on the sky. Therefore, without a true 2-dimensional image, the comparatively faint signal of any dust ring will be difficult to decipher against the spatial structure created by the K- and F-coronae and the solar streamers. The new generation of large format imaging infrared arrays is ideally suited to untangle the different components, search for the dust rings, and study the spatial structure of the infrared corona.

2. Observations

The observations were made at the NASA Infrared Telescope Facility (IRTF) on Mauna Kea during the July 11, 1991 solar eclipse. The camera, a modified Amber Engineering 'Infrared Imaging System', used a 128×128 InSb array with a 3.8-cm, f/2 lens, which produced a 4.9 degree field of view. The filter set included a 1.65 and 2.2 μm filter; a cold 2.5 μm thermal-blocking filter was also used. The camera, mounted on a portable solar tracker, was located on the eastern loading dock of the IRTF. The orientation of the InSb array was rotated to position the cardinal points along the 45 degree diagonals of the array. This orientation increased the radial distance along the ecliptic plane to 14 $R_{\odot}$. In addition, this orientation minimized any possible contamination of the solar signal by unknown row- or column-dependent fixed pattern noise sources.

During the four minutes of totality, the observations were divided into two 2-minute long intervals, one for the 1.65 μm filter and the other for the 2.2 μm filter. Only the 1.65 μm observations are presented in this paper. The 1.65 μm observations were divided into one minute of data taken at a frame rate of 1.69 frames/sec and another minute of data taken at data rates varying from 3 to 54 frames/sec. The data at 1.69 frames/sec produced the best images of the outer corona, but saturated most of the K-corona. The faster frame rates where required to obtain unsaturated images.

As a further precaution against contamination by fixed-pattern noise and dead, hot, or excessively noisy pixels, the image of the Sun was allowed to slowly drift southward across the array, and after each 30 second interval, the image of the Sun was quickly stepped by several pixels to the south. By doing so, as many different pixels as possible imaged the same region of the corona.

For each set of frames with different frame rates the data reduction included flat-fielding, bad pixel restoration, image shifting, and co-addition of the individual frames in each set. The absolute calibration was obtained by observing α Lyra on the night of July 11-12 and by laboratory observations of a calibrated blackbody. The two methods agreed to about 5 percent.

3. Results

The eclipsed Sun at 1.65 μm looks very similar to that seen at visible wavelengths. The K- and the F-corona and the solar streamers are clearly seen. But, as is shown in Fig. 1, no obvious dust rings are evident. This figure shows a plot of the surface

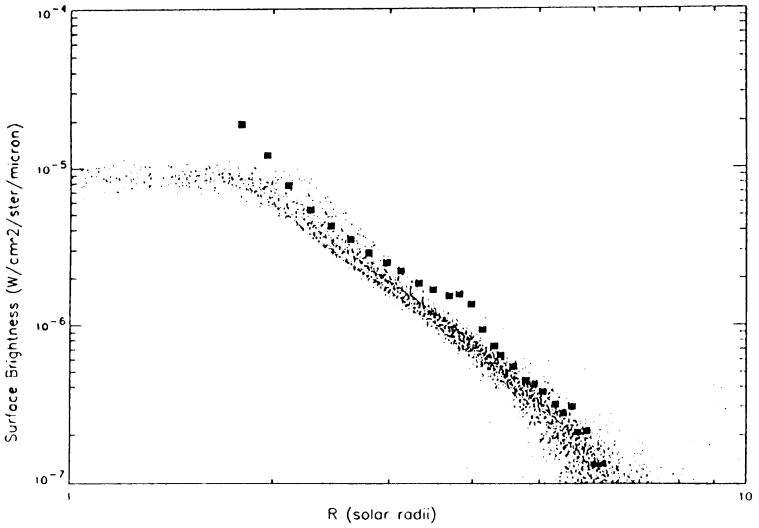

Fig. 1. A plot of surface brightness vs radial distance for each pixel in the co-added 0.6 sec, 1.65 μm image (dots). The large square symbols are the 1.65 μm data points from Mizutani *et al.* (1984). Below a radius of $2R_\odot$ the data is saturated.

brightness of each pixel versus the radial distance of that pixel. For reference, the 1.65 μm results from the 1983 solar eclipse (Mizutani *et al.* 1984) are over-plotted as large square symbols. Although the underlying corona from the two eclipses is nearly the same, no emission peak as bright as that seen in 1983 is evident in our 1991 eclipse.

Any faint dust ring signature would be difficult to detect on top of the very steep and bright corona. Therefore, we modeled the surface brightness of the F-corona, using an empirically determined model, and subtracted this signal from the observed signal. The empirical model was $S(R,\theta) = a + b(\theta)(R/R_\odot)^c$, where a compensates for zero-point offsets and b is dependent on polar angle θ. No physics is implied by the choice of this model; its sole purpose is to uniformly subtract off a reasonable approximation for the F-corona so that small scale fluctuations can be detected on the corona.

The model was determined by examining thin radial cuts at many different position angles around the sun (chosen to avoid the solar streamers). An example of how well this model worked is shown in Fig. 2, which shows a radial cut out the north pole and overplots the model fit. Also included is a plot of the residual signal after subtraction. The plots of the residual signal showed 4 features: 1) the K to F-corona transition region, which occurs abruptly at $2.5R_\odot$, 2) the best value of the power law, which was $c = 2.7 \pm 0.3$, 3) the total noise, which is about 2×10^{-7} W/cm^2/ster/μm peak-to-peak, and 4) the completeness of the F-coronal subtraction, although some nonzero signal is apparent at a level of 5×10^{-8}

https://doi.org/10.1017/S0074180900124416 Published online by Cambridge University Press

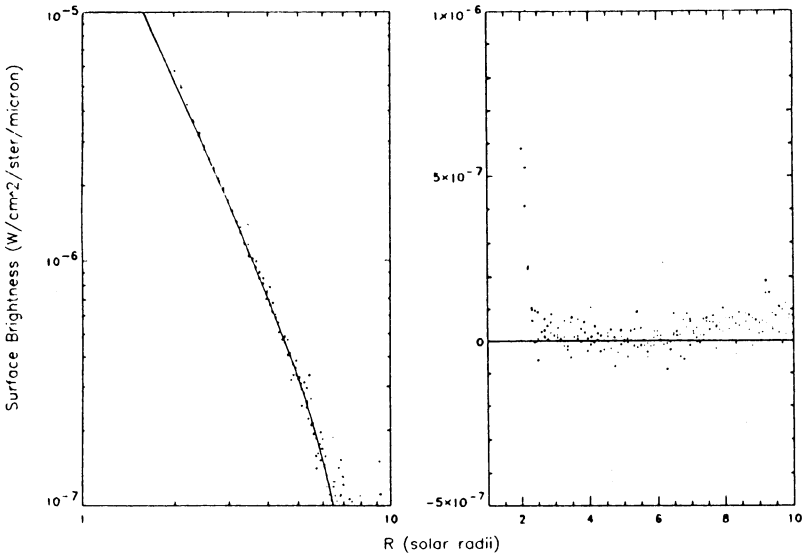

Fig. 2. The left plot compares the model coronal profile (line) to the data (dots) for a radial cut out the north pole. The right-hand plot shows the residuals after the model is subtracted from the real data.

W/cm^2/ster/μm. Another general result is that the equatorial regions are 15% brighter than the polar regions.

After subtracting the model from the real data, an image of the residual signal showed two faint emission peaks, one located on each side of the sun, along the ecliptic, and at about $4R_\odot$. No other similarly shaped peaks are apparent, the only other remaining features are the solar streamers and the saturated inner regions of the K-corona. Fig. 3 shows four plots that compare cuts through the east with cuts through the north and south, and similar comparisons for a western cut. In all four comparisons, excess emission is apparent in both the east and the west cuts (as compared to the north or south cut) for radial distances between 3.5 and $4.5R_\odot$. The excess emissions are too faint to definitively state that dust rings exist, but their presence is apparent, as illustrated in Fig. 3. They are equally spaced, and lie along the east-west plane at a radius of about $4R_\odot$. Only half of the data has been reduced, so any further conclusions must be deferred until after all of the data is completely analyzed.

Acknowledgements

The authors were Visiting Astronomers at the IRTF which is operated by the University of Hawaii under contract from the National Aeronautics and Space Ad-

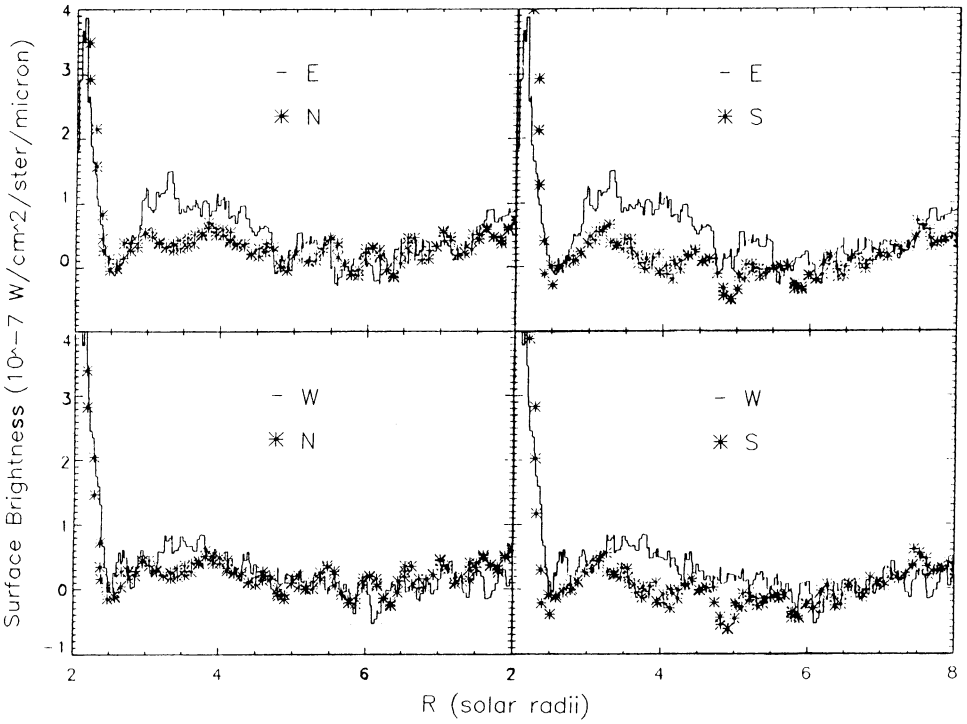

Fig. 3. The four plots compare radial cuts in the east or west direction (lines) to cuts in the north or south direction (stars) of the residual signal that remains after the model signal is subtracted from the real data. The data has been smoothed with a 3 pixel wide box-car filter to dampen the high spatial frequency noise.

ministration. We wish to thank Amber Engineering for their financial and technical support of this experiment, as well as their generous loan of a 128×128 InSb Infrared Imaging System and the National Solar Observatory for the loan of the solar tracker.

References

Isobe, S., Hirayama, T., Baba, N., and Miura, N.: 1985, *Nature* **318**, 644.
Lena, P., Viala, Y., Hall, D., and Soufflot, A.: 1974, *Astron. Astrophys.* **37**, 81.
MacQueen, R. M.: 1968, *Astrophys. J.* **154**, 1059.
Mankin, W. G., MacQueen, R. M., and Lee, R. H.: 1974, *Astron. Astrophys.* **31**, 17.
Mizutani, K., Maihara, T., Hiromoto, N., and Tamaki, H.: 1984, *Nature* **312**, 134.
Peterson, A. W.: 1967, *Astrophys. J. (Letters)* **148**, L37.
Peterson, A. W.: 1969, *Astrophys. J.* **155**, 1009.
Peterson, A. W.: 1971, *Bull. Amer. Astron. Soc.* **3**, 500.
Rao, U. R., Alex, T. K., Iyengar, V. S., Kasturirangan, K., Marar, T. M. K., Mathur, R. S., and Sharma, D. P.: 1981, *Nature*, **289**, 779.